Temperature and hydroxyl radical abundance limit the photochemical degradation kinetics and photoproducts of fluridone in high-latitude aquatic systems

Brian DiMento*, Isabel Hillestad, Julie Sommer, Aidan Pavia, Niquelina Smith, Patrick Tomco, Zachary Redman

Department of Chemistry, College of Arts and Sciences, University of Alaska Anchorage, 3211 Providence Dr., Anchorage, AK 99508, United States
*Address correspondences to: bpdimento@alaska.edu

TOC Graphic

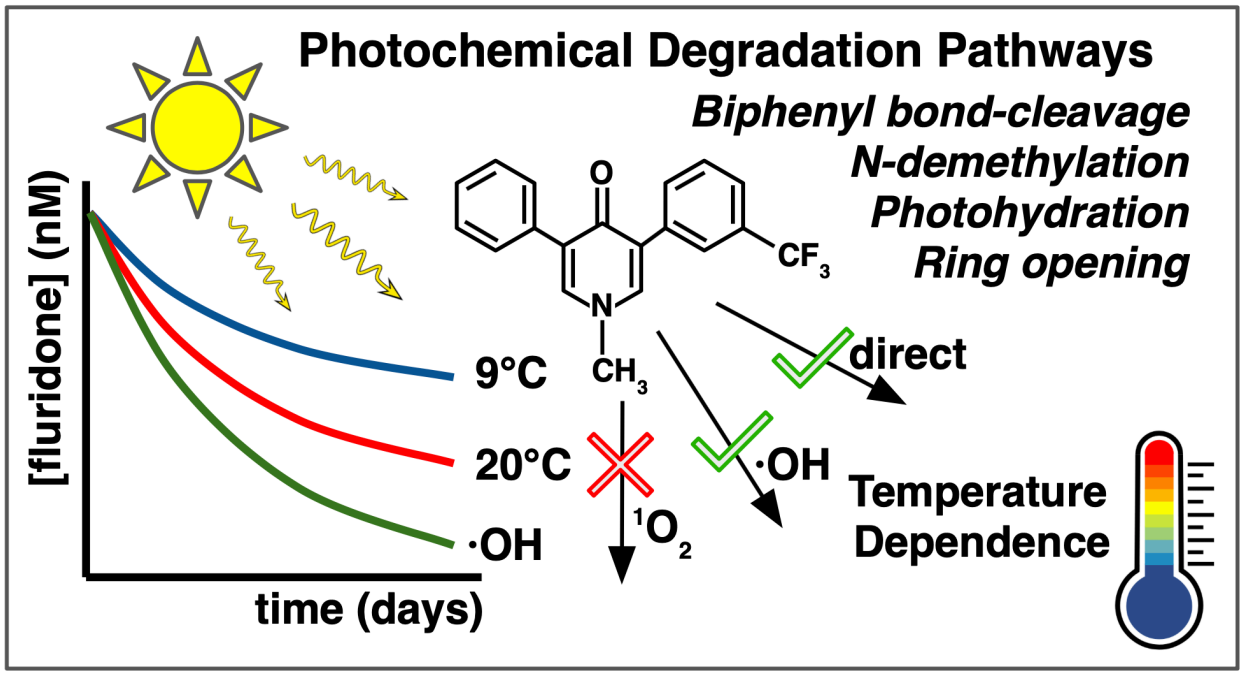

Abstract

Temperature is often overlooked as an environmental driver of aquatic pollutant photodegradation kinetics; however, it may strongly impact contaminant persistence in polar climates characterized by low summertime temperatures and near-continuous sunlight. The photochemical degradation of fluridone (FLU), an herbicide applied worldwide to waterways for the eradication of invasive freshwater species, was investigated under simulated sub-arctic conditions typical of high-latitude surface waters. Temperature had a strong effect on the photochemical degradation of FLU, with half-lives for direct photochemical degradation ranging from approximately 40 h at 22 °C to 118 h at 9 °C under constant irradiation. Assessment of

indirect processes involving reactive oxygen species indicated that FLU will primarily react with hydroxyl radicals (·OH) and not singlet oxygen ($^1O_2$) produced by chromophoric dissolved organic matter (CDOM) in the environment. These results were corroborated by Fenton experiments, resulting in a calculated second order rate constant for the reaction with ·OH of 8.37×10^9 M^{-1} s^{-1}. Photoproduct identification revealed four main pathways for direct and indirect FLU photodegradation. Taken together, this work shows that direct photochemical degradation, which is dominant, is temperature dependent. Also, the interplay between light screening and ·OH production of environmental CDOM, which is site dependent, will strongly influence FLU persistence.

Keywords

Hydroxyl radical, singlet oxygen, photolysis, photochemistry, transformation products, non-target analysis

Synopsis

The persistence of aquatic pesticides in polar climates is poorly understood. This study reports the kinetics and reaction mechanisms of fluridone photodegradation under environmentally relevant temperatures and light regimes.

Introduction

In regions of the circumpolar North, persistence of environmental pollutants is a well-established issue due to the presence of cold temperatures[1–5]. Long residence times of anthropogenic pollutants can cause chronic exposure to sensitive aquatic species, leading to bioaccumulation of lipophilic toxicants. Therefore, the accurate forecasting of aquatic persistence is paramount for managing water quality where pesticides are applied.

Fluridone (CAS 59756-60-4, FLU, Figure 1) is an herbicide applied to eradicate freshwater macrophytes across the world. The application of FLU in high-latitude regions such as Alaska is relatively new and has rapidly increased in popularity as climate change is affecting invasive species proliferation in the sub-Arctic at alarming rates[6,7] [X]. For instance, *Elodea canadensis* has proliferated significantly, to the potential detriment of the world's largest salmon stocks in Alaska[8]. While FLU is seen as essential in combating invasive plants, FLU is significantly more persistent in Alaska than in temperate climates; previous treatments in Alaskan lakes noted >50% of initial applied herbicide existed 2 years following treatment[9], still at toxic levels. Low photochemical degradation rates and cold water temperatures were postulated as the most likely driver of the long residence times[9], but no studies have verified this. Therefore, the fundamental photochemical behavior of FLU is of high interest in high-latitude regions. Despite this acknowledgment by the manufacturer, no study to-date has identified the temperature-dependent behavior of photochemical degradation, and which photochemical pathways drive these kinetics.

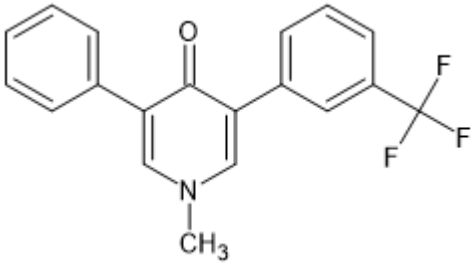

Figure 1. Structure of the aquatic herbicide fluridone (CAS 59756-60-4, FLU). Molecular formula: $C_{19}H_{14}F_3NO$, K_{OW}= 74 (20 ºC), Water solubility: 12 mg/L (pH 7, 25 ºC), pKa: 12.3[10].

Aquatic contaminants are known to photochemically degrade via direct and indirect pathways. Direct photodegradation requires absorption of a photon by a molecule to induce excitation and a chemical reaction. The direct photochemical pathway may also include intersystem crossing to a triplet excitation state prior to decomposition, which can be influenced by other indirect quenching or sensitizing processes. Indirect photodegradation is described by numerous degradation pathways in which the contaminant reacts with photon-induced reactive transient species such as hydroxyl radical (·OH), singlet oxygen ($^1O_2$), or triplet state chromophoric dissolved organic matter (^{3}CDOM*). As environmental factors such as temperature, dissolved oxygen, and CDOM character vary across surface waters, the observed degradation kinetics for FLU can be site-specific and difficult to predict[11]. While previous studies have investigated the direct photochemical properties of FLU under laboratory settings[12,13], indirect processes have been relatively understudied and advances in non-target analysis using high-resolution mass spectrometry now enable a robust analysis of degradation pathways.

The overall goal of this work was to assess the temperature dependence of direct and indirect FLU photo-degradation pathways under simulated high-latitude summertime solar conditions. Further, we aimed to detect and identify the primary photoproducts formed. This was accomplished by illuminating solutions of FLU in the presence of probe molecules that isolate the contributions of ·OH, $^1O_2$, and ^{3}CDOM*.

Materials and Methods

Details regarding all chemical reagents used can be found in the Supporting Information (Section S1).

2.1 Molar Absorptivity

High-performance liquid chromatography with diode array detection was used to measure the molar absorptivity of FLU ($\varepsilon_{FLU,\lambda}$; M^{-1} cm^{-1}) as previously reported[14–16]. Briefly, 10 µL of solutions containing 500, 250, 80, 65, 35, and 10 µM FLU in methanol and water (80:20, v/v) were injected into an InfinityLab Poroshell 120 EC-C18 column (3.0 x 50 mm; 2.7 µm) and eluted isocratically with methanol and water (50:50, v/v) at a flow of 0.3 mL/min. The retention time of FLU was 5.2 min. Absorbance spectra (205-800 nm) were recorded and blank spectra

were subtracted prior to baseline correction. Molar absorptivity was calculated as the slope of the line obtained from Eq 1

$$\text{area}_{\lambda} = \varepsilon_{FLU,\lambda} \cdot (b \cdot N \cdot 6 \times 10^{-7})/F \quad (1)$$

where area_{λ} is the peak area (mAU s) for wavelength λ (nm), b is the path length (cm), N is the moles of FLU injected, F is the flow rate, and 6×10^{-7} combines the conversions from seconds to minutes, mAU to AU, and mL to L. The peak area for each wavelength was calculated using eq 2:

$$\text{area}_{\lambda} = A_{\lambda} \cdot \Delta t \cdot (A_{237} \cdot \Delta t)/\text{measured peak area for 327 nm} \quad (2)$$

where A_{λ} is the absorbance (mAU) at wavelength λ, A_{237} is the absorbance at 327 nm, and Δt is the chromatographic peak width (s).

2.2 Degradation Experiments

The rate of FLU direct photochemical degradation under simulated solar radiation was determined using microcosms (n = 4) containing 50 nM FLU in phosphate buffered water (5 mM, pH 7) with 0.1% acetonitrile (v/v). Additional microcosms (n = 4/treatment) were prepared containing probe molecules in phosphate buffered water (5 mM, pH 7). Details for each experiment, including the SunTest XLS+ solar simulator, are provided in the Supporting Information (Section S2). The position-corrected first-order rate constants (j, h^{-1}), half-lives ($t_{1/2}$, h), and apparent quantum yields (ϕ, AQY) for the photochemical degradation of FLU were calculated for each treatment according to eq. 3-5:

$$\ln(C_t/C_0)/F_P = jt \quad (3)$$

$$t_{1/2} = \ln(2)/j \quad (4)$$

$$\phi = (j\, \Sigma[\varepsilon_{2NB,\lambda}\, I_{\lambda}])/(j_{2NB}\, \Sigma[\varepsilon_{FLU,\lambda}\, I_{\lambda}])\, \phi_{2NB} \quad (5)$$

where C_0 and C_t are the initial concentration (nM) and concentration of FLU at time t (h), respectively, F_P is the actinometry correction factor, I_{λ} is the volume averaged photon flux (mol photons L^{-1} s^{-1}) at wavelength λ (nm), and ϕ_{2NB} is the quantum yield for the photoisomerization of 2NB (ϕ_{2NB} = 0.41)[17]. Rate constants from SRFA and SRHA containing treatments were corrected for light screening by CDOM using eq. 6-8:

$$S_{\lambda} = (1\text{-}10^{-\alpha\lambda l}) / (2.303\, \alpha_{\lambda}\, l) \quad (6)$$

$$S_{w,280\text{-}365} = \Sigma_{280\text{-}365}[S_{\lambda} \cdot (I_{\lambda}/\Sigma_{280\text{-}365} I_{\lambda})] / \Sigma_{280\text{-}365}[I_{\lambda}/\Sigma_{280\text{-}365} I_{\lambda}] \quad (7)$$

$$j_{S\ corrected} = j / S_{w,280\text{-}365} \quad (8)$$

where S_λ is the screening factor at wavelength $\boldsymbol{\lambda}$ (nm), α_λ is the pathlength-normalized absorbance of the solution, l is the pathlength (cm), and $S_{w,280\text{-}365}$ is the weighted average screening factor for the wavelength range 280-365 nm (the range for which FLU absorbs light).

The activation energy (E_a; kJ mol^{-1}), enthalpy of activation ($\Delta H^{\ddagger}$; kJ mol^{-1}), and entropy of activation ($\Delta S^{\ddagger}$; J mol^{-1} K^{-1}) for direct, nitrate, and SRFA microcosms were calculated from the slope of the Arrhenius equation (eq. 9), slope of the Eyring equation (eq. 10), and intercept of the Eyring equation, respectively.

$$\ln j = -E_a/RT + \ln A \quad (9)$$

$$\ln(j/T) = -\Delta H^{\ddagger}/RT + \ln (k_b/h) + \Delta S^{\ddagger}/R \quad (10)$$

where T is the temperature (K), R is the ideal gas constant (J mol^{-1} K^{-1}), k_b is Boltzman's constant (J K^{-1}), and h is Planck's constant (J s).

Supplementary experiments (n = 4/treatment) were conducted to determine the contributions of ·OH and $^1O_2$ in the dark (Section S2). The second order rate constant for the reaction of FLU with ·OH ($k_{FLU,\cdot OH}$; M^{-1} s^{-1}) was determined from the slope of the line obtained by plotting eq. 11[18,19]

$$\ln([FLU]_t/[FLU]_0) = (k_{FLU,\cdot OH}\ k_{PhOH,\cdot OH}) \ln([PhOH]_t/[PhOH]_0) \quad (11)$$

where $k_{PhOH,\cdot OH}$ is the reported second order rate constant for the reaction of phenol with ·OH (6.6×10^9 M^{-1} s^{-1})[20].

Action spectra for the direct photochemical degradation of FLU (with and without light screening by SRFA and SRHA CDOM surrogates) in the solar-simulator used in this experiment were calculated using eq. 12.

$$j_\lambda = 2.303 \cdot l \cdot \varepsilon_{FLU} \cdot \boldsymbol{\phi} \cdot I_\lambda \quad (12)$$

The theoretical steady state concentration of ·OH ($[\cdot OH]_{ss}$; M) necessary to overcome light screening by CDOM was calculated assuming an overall first order rate constant from eq. 13.

$$j_{total} = \Sigma j_\lambda \cdot S_\lambda + k_{FLU,\cdot OH}[\cdot OH]_{ss} \quad (13)$$

Quantitative methods for FLU, PhOH, and 2NB are provided in the Supporting Information (Section S3). All rate constants, half-lives, and AQY are presented as the average ± standard deviation (n = 4/experimental treatment, n = 3/control treatment). Statistical differences were evaluated via analysis of variance (ANOVA) with a Wilk-Shapiro test to confirm the assumption of normally distributed residual error (W > 0.9) and posthoc Tukey honest significant difference (HSD) comparisons (α = 0.05) using JMP Pro 16 (SAS Institute, Cary, NC).

2.3 Nontarget Photoproduct Identification

Degradation experiments for buffered direct and nitrate (1 mM) microcosms (n = 3/time point/treatment) of FLU (1 μM) were repeated at 22 °C and the entire volume of each sample (15 mL) was concentrated via Hydrophilic-Lipophilic-Balance solid phase extraction (SPE, Waters Oasis HLB, 500 mg, 6mL). Photoproducts were identified via a non-targeted analysis using ultra-high-performance liquid chromatography with high-resolution Orbitrap mass spectrometry (UHPLC-Orbitrap). The experimental details for sample collection, solid phase extraction, and UHPLC-Orbitrap analysis parameters are available in the Supporting Information (Section S4).

Results and Discussion

3.1 Molar Absorptivity and Direct Photochemical Degradation.

Molar absorptivity and all first-order rate constants for the degradation of FLU in this study are tabulated in the Supporting Information (Tables S5 and S6). FLU has a single broad absorption peak in the solar range, extending from 290 to 366 nm and peaking at 300 nm (ε_{300} = 12298 M^{-1} s^{-1}) (Figure 2a, Table S5). Van Frost et al. (2024) also reported a broad absorption peak overlapping with the solar spectrum, peaking at 282 nm (ε_{282} ≈ 11000 M^{-1} s^{-1}, ε_{300} ≈ 9700 M^{-1} s^{-1}), consistent with previous observations that FLU will photodegrade when exposed to light of wavelength less than 400 nm, and particularly less than 325 nm[12,13].

The direct aqueous photochemical degradation of FLU was slow, with a measured half-life of 39.8 ± 0.9 h (j = 0.0174 ± 0.0004 h^{-1}) at 22 °C. Neither addition of Cs^+ (100 mM, $t_{1/2}$ = 39.0 ± 1.2 h, j = 0.0178 ± 0.0005 h^{-1}) to promote intersystem crossing nor the triplet sensitizer 2-acetonaphthone (2-AN, 10 μM, $t_{1/2}$ = 39.7 ± 1.1 h, j = 0.0175 ± 0.0005 h^{-1}) resulted in a significant change in the photochemical degradation of FLU. This may be the result of rapid forward and reverse intersystem crossing as observed for other pyridinone compounds, such as acridones[21]. However, a slight yet significant increase in the rate was observed following argon purging ($t_{1/2}$ = 31.9 ± 3.0 h, j = 0.0219 ± 0.0021 h^{-1}) (Figure 2b), consistent with Saunders and Mosier (1983) in nitrogen purged water[22]. No degradation was observed in dark controls. Taken together, these results indicate that intersystem crossing is minor and that the primary pathway for the direct photochemical degradation of FLU proceeds from the singlet excitation state with an apparent quantum yield of 1.20(±0.03)x10^{-4} at 22 °C. Previously reported quantum yields ranged from 2.7x10^{-5} under UV-A irradiation[22] to 3.8x10^{-4} at 311 nm[11]. Results from this study fall within this range, with differences likely attributable to variability in irradiation wavelengths and temperature (*vide infra*, Section 3.2) between experiments.

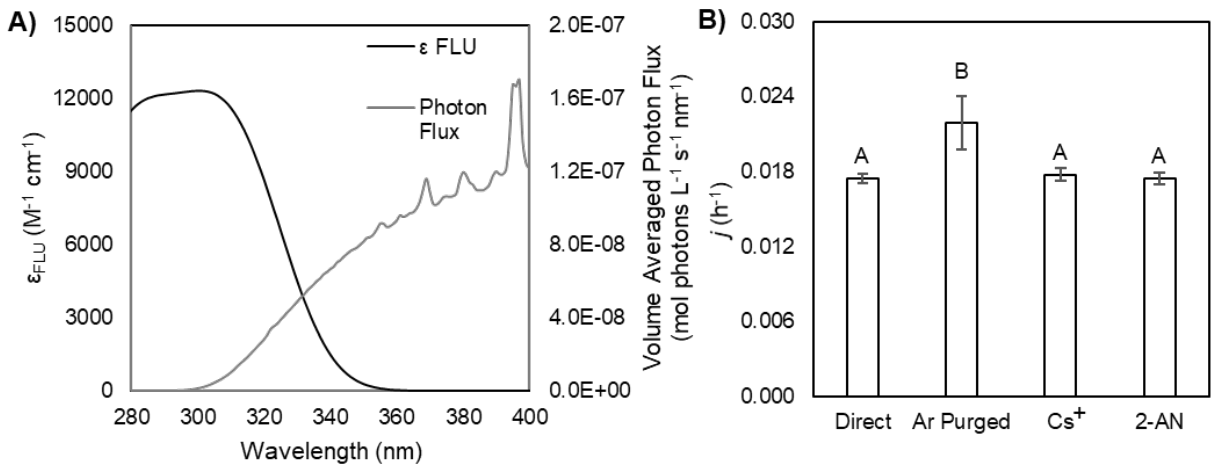

Figure 2. A) Molar absorptivity (ε, M^{-1} cm^{-1}) for FLU and the volume averaged photon flux (mol photons L^{-1} s^{-1} nm^{-1}) for the SunTest XLS+ solar simulator. **B)** Pseudo first order rate constants (h^{-1}, average, error bars represent one standard deviation, n = 4) for the direct and triplet sensitized (Ar purged, 100 mM Cs^+, 10 µM 2-AN) photochemical degradation of FLU (50 nM). Statistical differences ($p < 0.05$, Tukey HSD) are denoted by different letter labels (A & B).

3.2 Temperature Dependence

Temperature had a direct effect on the photochemical degradation of FLU, with the half-life for direct photochemical degradation decreasing from 39.8 ± 1.2 h (j = 0.0174 ± 0.0004 h^{-1}) at 22 °C to 118.2 ± 8.4 h (j = 0.0059 ± 0.0004 h^{-1}) at 9 °C, corresponding to apparent quantum yields of 1.2 x 10^{-4} ± 2.8 x 10^{-6} and 4.3 x 10^{-5} ± 3.0 x 10^{-6} (Figure 3a). The direct relationship between temperature and photochemical degradation indicates that absorbance from a higher vibrational level in the electronic ground state increases the probability of bond dissociation upon excitation to the singlet state; similar to the simplified example provided by the potential energy curves for the photo-dissociation of chlorine[23]. With respect to FLU, temperature likely accelerates the cleavage of the biphenyl bonds (*vide infra*, Section 3.4) as these bonds, having the least double bond character, are more likely to reach higher vibrational levels in the ground state and promote photo-dissociation. Similarly, photochemical half-lives decreased from 21.3 ± 0.6 h (j = 0.0326 ± 0.0009 h^{-1}) at 22 °C to 48.4 ± 2.2 h (j = 0.0144 ± 0.0006 h^{-1}) at 9 °C and 27.6 ± 0.6 h (j = 0.0252 ± 0.0006 h^{-1}) at 22 °C to 63.1 ± 5.1 h (j = 0.0110 ± 0.0009 h^{-1}) in nitrate and SRFA containing microcosms, respectively.

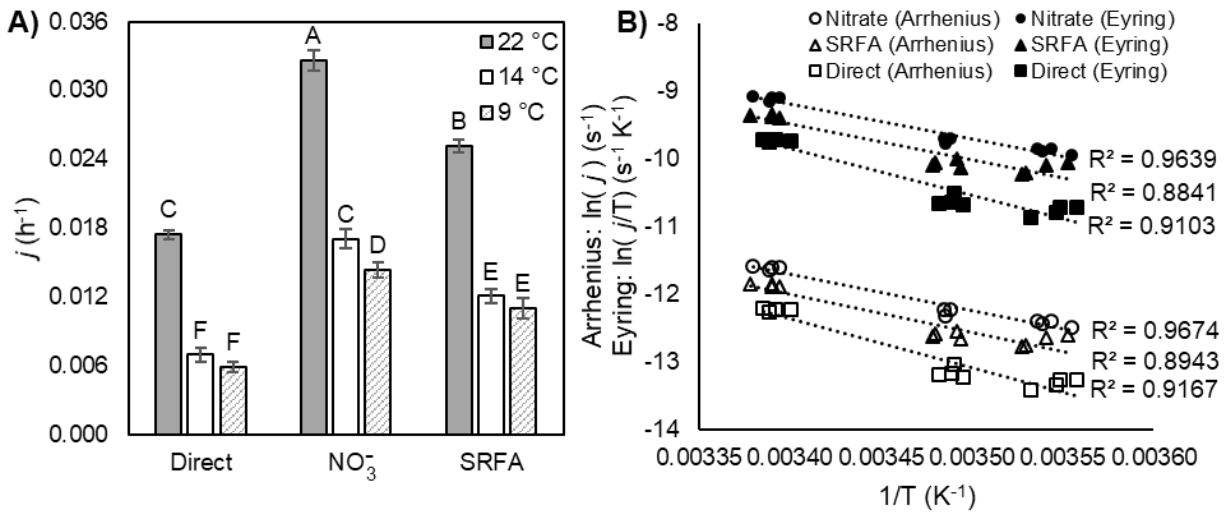

Figure 3. A) Average pseudo first order rate constants (*j*, h^{-1}, error bars denote one standard deviation, n = 4) for the photochemical degradation of FLU in direct, NO_3^- (1 mM), and SRFA (10 mg L^{-1}) microcosms at 22 (gray bars), 14 (open bars), and 9 °C (hashed bars). Statistical differences ($p < 0.05$, Tukey HSD) are denoted by different letter labels (A - C). **B)** Arrhenius (black symbols) and Eyring (open symbols) plots for the temperature dependent degradation in direct (squares), NO_3^- (circles), and SRFA (triangles) microcosms.

Calculated apparent activation energies for the degradation of FLU in nitrate (45 kJ mol^{-1}) and SRFA (47 kJ mol^{-1}) microcosms were 13 - 15 kJ mol^{-1} lower than the measured activation energy for the direct photochemical degradation of FLU (60 kJ mol^{-1}) (Figure 3B & Table S4). Apparent activation energies do not precisely measure the reaction of ·OH with FLU as activation energies reported for the production of ·OH by both nitrate (16 ± 4 - 19 ± 4 kJ mol^{-1}) and SRFA (34.3 ± 7.2 kJ mol^{-1}) confirm some temperature dependence for the production of ·OH in these systems[24–26]. Nevertheless, similar activation energies for FLU degradation in the presence of nitrate and SRFA suggest a similar degradation mechanism, further supporting the conclusion that reaction with ·OH will be the primary indirect pathway for degradation when CDOM is involved. Similar trends were observed for the enthalpies of activation; however, the magnitude of the entropies of activation for the degradation of FLU by ·OH (-130 and -125 J mol^{-1} K^{-1} for nitrate and SRFA, respectively) was much larger than that measured for its direct photodegradation (-85 J mol^{-1} K^{-1}) (Table S7). The similarities between the two indirect systems further support the case for a similar degradation mechanism and their discrepancy from direct photodegradation may be attributable to the increased complexity of the indirect degradation mechanisms added by the production of ·OH rather than $^1O_2$, which was not observed to react with FLU (*vide infra*, Section 3.3).

3.3 Indirect Photochemical Pathways

Follow-on experiments utilized select quenching and sensitizing reagents to investigate the contribution of the reactive oxygen species $^1O_2$ and ·OH to the indirect photochemical degradation of FLU. The photochemical degradation of FLU was enhanced in the presence of

nitrate (1 mM, $t_{1/2}$ = 21.3 ± 0.6 h, j = 0.0326 ± 0.0009 h^{-1}) as well as SRFA (10 mg L^{-1}, 4.5 mgC L^{-1}, $SUVA_{254}$ = 4.4 L mg^{-1} m^{-1}; $t_{1/2}$ = 30.0 ± 0.7 h, j = 0.0231 ± 0.0005 h^{-1}) and SRHA (10 mg L^{-1}, 5.4 mgC L^{-1}, $SUVA_{254}$ = 5.3 L mg^{-1} m^{-1}; $t_{1/2}$ = 28.3 ± 0.7 h, j = 0.0245 ± 0.0006 h^{-1}) after correction for light screening ($S_{wSRFA,280-365}$ = 0.8788, $S_{wSRHA,280-365}$ = 0.7892, Figure 4a). Before light screening correction, FLU degradation was not significantly accelerated in SRHA microcosms. These results indicate that the interplay between light screening and ·OH production by CDOM may have a significant impact on the persistence of FLU in the environment. Addition of either isopropanol (IPA, 25 mM) as a ·OH scavenger or azide (1 mM) as a $^1O_2$ quencher to SRFA ($t_{1/2}$ = 36.0 ± 1.3 h, j = 0.0192 ± 0.0007 h^{-1} and $t_{1/2}$ = 33.7 ± 0.9 h, j = 0.0206 ± 0.0005 h^{-1}, respectively) and SRHA ($t_{1/2}$ = 34.6 ± 0.5 h, j = 0.0200 ± 0.0003 h^{-1} and $t_{1/2}$ = 31.9 ± 0.9 h, j = 0.0217 ± 0.0006 h^{-1}, respectively) microcosms reduced the rate of FLU degradation. A greater reduction to the degradation rate with the addition of IPA, along with the enhanced degradation rate with the addition of nitrate, support the conclusion that the presence or absence of ·OH in the environment may significantly alter the persistence of FLU. Direct photochemical degradation of FLU was not significantly altered by the addition of IPA ($t_{1/2}$ = 42.5 ± 0.8 h, j = 0.0163 ± 0.0003 h^{-1}) while dark Fenton experiments (Figure 4b) revealed rapid FLU degradation. The second order reaction rate constant, calculated relative to the degradation rate of phenol (6.60 x 10^9 M^{-1} s^{-1})[20], was 8.4(±0.9)x10^9 M^{-1} s^{-1}. No degradation was observed with the addition of only Fe(II) or hydrogen peroxide at pH 3. While FLU was observed to react with nitrate radical at the elevated concentration of FLU used for photoproduct identification (*vide infra,* Section 3.4), Fenton experiments confirmed that reaction with ·OH is a significant reaction pathway.

FLU degradation was not observable in the presence of $^1O_2$ generated by MoO_4^{2-} and H_2O_2, suggesting that $^1O_2$ does not contribute to the degradation of FLU. Addition of azide, however, resulted in a statistically significant reduction in the direct photochemical degradation rate ($t_{1/2}$ = 45.7 ± 1.3 h, j = 0.0152 ± 0.0004 h^{-1}). It is plausible for azide ($E_{1/2}$ $\cdot N_3/N_3^-$ = 1.32 V) to reduce the hypothetical radical cation formed by the photoionization of FLU[27] (see discussion in Section 3.4) to form the azide radical and regenerate FLU[28–32], or quench FLU excited states based on previous observations of 2-phenyl benzoxazole fluorescence[33]. Notably, a similar decrease in the direct photochemical degradation of FLU was observed in deuterium oxide ($t_{1/2}$ = 46.6 ± 0.9 h, j = 0.0149 ± 0.0003 h^{-1}). The observed kinetic solvent isotope effect (KSIE; j_H/j_D = 1.17) may be attributable to an inhibition of photo-hydration[34] or a proton coupled electron transfer involving the radical cation discussed below (Section 3.4); however, neither mechanism can be confirmed via the steady state experiments and photoproduct identification performed in this work. A non-singlet oxygen based KSIE was previously observed to enhance the photochemical degradation of diaryl amines via inhibition of radical cation reduction via H/D coupled electron transfer with DOM phenols[35]. While separate mechanisms for the KSIE are proposed for the direct photochemistry of FLU in this work than that previously described for the photochemistry of diaryl amines, these results reinforce that caution be taken when using KSIE for the interpretation of photochemical pathways potentially involving radical cation amines.

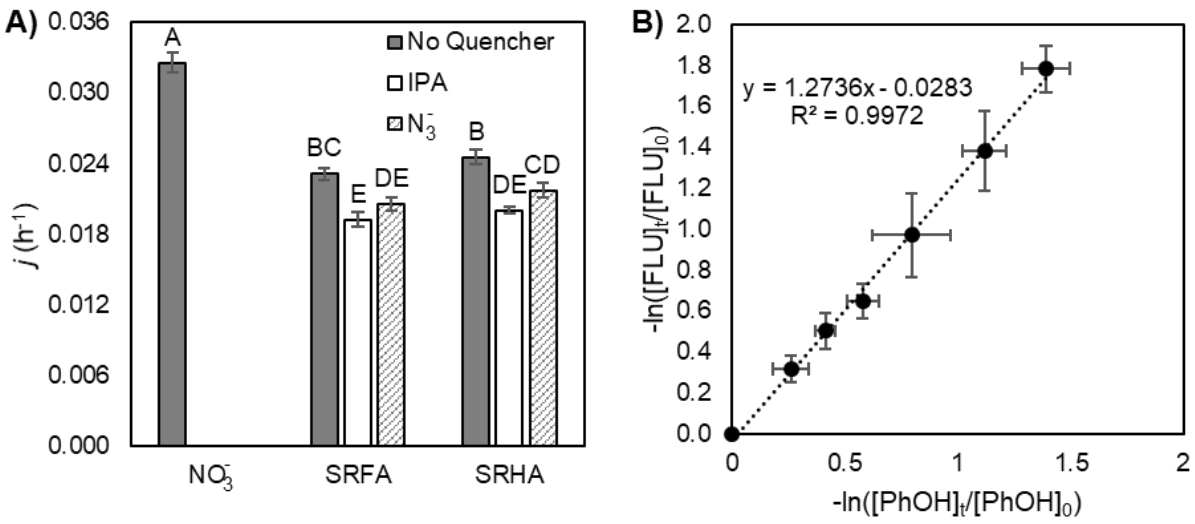

Figure 4. A) Average pseudo first order rate constants (j, h^{-1},, error bars represent one standard deviation, n = 4) for the degradation of FLU (50 nM) in the presence of NO_3^- (1 mM) as a ·OH sensitizer and SRFA or SRHA (10 mg L^{-1}) CDOM surrogates with or without IPA (25 mM) and azide (5 mM) as quenchers. Results presented for SRFA and SRHA are corrected for light screening. Statistical differences (p < 0.05, Tukey HSD) are denoted by different letter labels (A - E). **B)** Natural log linearized plot of the relative concentrations for FLU (1 µM) and PhOH (10 µM) in the Fenton reaction microcosms. Points represent averages with error bars in the x and y representing one standard deviation for the natural log transformed relative concentrations (n = 4). The average second order rate constant for the reaction of FLU with ·OH calculated from the slope of each replicate was 8.4(±0.9)x10^9 M^{-1} s^{-1}.

The molar absorptivity, AQY for the direct photolysis of FLU at 22 °C, and screening factors for SRFA and SRHA, were used to calculate the action spectra for FLU under the simulated solar light used in this work (Figure 5A). The single prominent absorption band (Figure 2A) and peak in the action spectrum (Figure 5A) indicate that the quantum yield for the direct photochemical degradation of FLU does not have a strong wavelength dependence. Therefore, the AQYs presented in this work under simulated solar conditions are sufficient for these calculations. The calculated half-life for the direct photochemical degradation of FLU (eq. 12) was 40 h and increased to 48 and 54 h with light screening by SRFA and SRHA. Based on the second order rate constant for the reaction of FLU with ·OH, the theoretical steady state concentrations of ·OH ($[\cdot OH]_{ss}$) required to overcome light-screening by SRFA and SRHA are 8.9x10^{-17} and 1.5x10^{-16} M, respectively (Figure 5B). Considering the steady state concentration of ·OH in natural waters typically ranges between 10^{-18}-10^{-15} M[36–40], it is possible for this indirect photochemical pathway to overcome light-shielding by CDOM depending upon the temperature dependent quantum yield for the production of ·OH by CDOM and the concentration of other ·OH scavenging species. However, because the quantum yield for ·OH by CDOM is not close to unity we can assume that it becomes increasingly unlikely that reaction with ·OH will accelerate the overall observed degradation rate of FLU as light screening is increased and temperature is decreased.

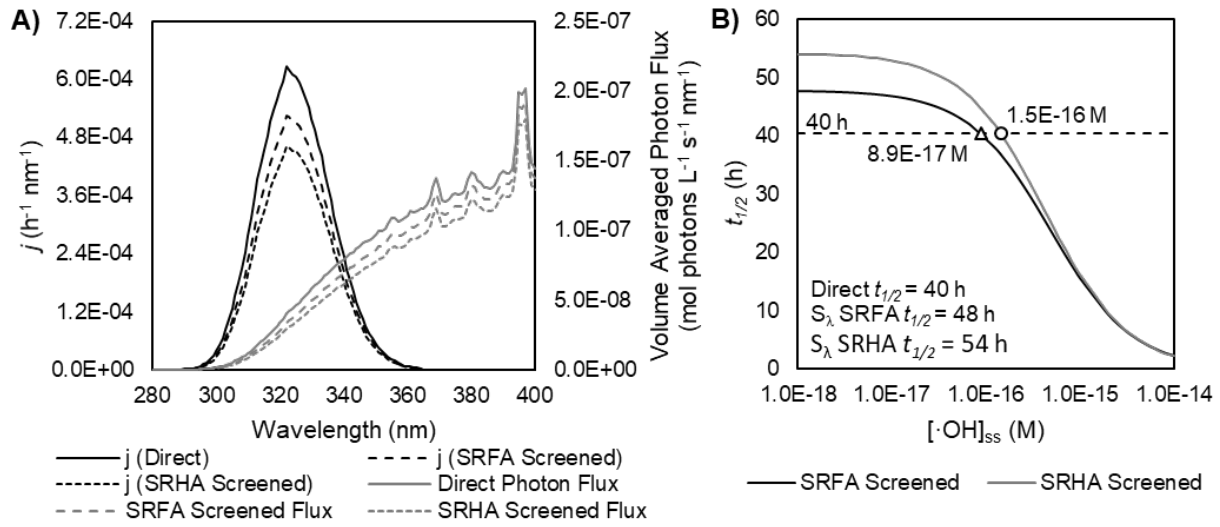

Figure 5. A) Action spectra for the direct photochemical degradation of FLU (black lines, s^{-1} nm^{-1}) and volume average photon flux (gray lines, mol photons L^{-1} s^{-1} nm^{-1}) with and without light screening by SRFA and SRHA at 22 °C. **B)** Calculated photochemical half-lives (h) for FLU in SRFA and SRHA screened solutions with varying $[\cdot OH]_{ss}$ (M). Open symbols denote the theoretical $[\cdot OH]_{ss}$ necessary to overcome light screening by SRFA (triangle, 8.9 x 10^{-17} M) and SRHA (circle, 1.5 x 10^{-16} M) at 22 °C.

3.4 Detection and Identification of Photoproducts and Degradation Pathways

Photochemical degradation products for the predominant photochemical pathways, direct and indirect reaction with hydroxyl radical were characterized. Structures are proposed with *up to* Level 2b: Probable Structure (Diagnostic) confidence, according to the framework established by Schymanski et al. (2014)[41]. Briefly, the proposed products are tentative candidates with unambiguous molecular formula (Level 4) and fragmentation data (Level 3) with evidence to support a proposed structure based on the known parent compound and experimental context (Level 2b). Details for each proposed transformation product, including structure, molecular formula, mass to charge ratio, mass error and retention time, are provided along with chromatograms, fragmentation spectra, and abundance over time in the Supporting Information for Transformation Products. Overall, 28 probable structures were identified that were consistent with the photodegradation of FLU through four primary transformation pathways: I) biphenyl bond cleavage α to the ketone, II) N-demethylation, III) photohydration and ring opening α to the nitrogen, and IV) ring opening of the phenyl rings (Figure 6, Supporting Information for Transformation Products).

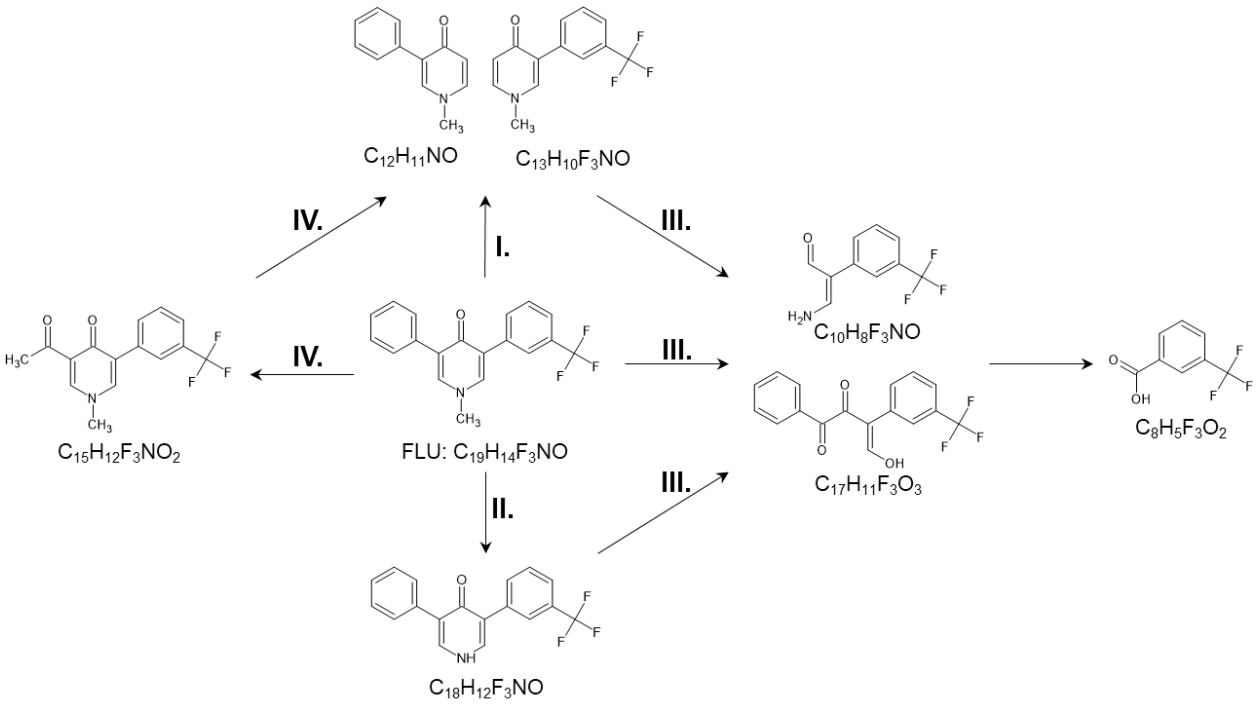

Figure 6. Primary FLU photochemical degradation pathways and representative intermediates identified via UHPLC-Orbitrap analysis. **I.** biphenyl bond cleavage α to the ketone, **II.** N-demethylation, **III.** photohydration and ring opening of the pyridinone ring, and **IV.** ring opening of the phenyl rings.

The primary photoproducts (or intermediates) identified in this study in both direct and nitrate treatments were $C_{12}H_{11}NO$ and $C_{13}H_{10}F_3NO$, indicating Pathway I: loss of phenyl and trifluoromethylphenyl groups after biphenyl bond cleavage α to the ketone (Figure 6) is a major pathway for both direct photolysis and reaction with ·OH. Notably, hydroxylated products of these intermediates were also observed to form in the presence of ·OH (Supporting Information for Transformation Products), indicating that bond scission may occur through homolytic cleavage followed by H abstraction or reaction with ·OH to form a stable intermediate. N-demethyl fluridone ($C_{18}H_{12}F_3NO$, Fig 6, Pathway II) was another major product observed during the direct photodegradation of FLU. This suggests that FLU may directly photoionize to a radical cation and demethylate following proton transfer and hydrolysis of the resulting imine[42–44]. While this work is the first to observe this pathway, likely due to the rapid degradation of the demethylated intermediate (Figure 7), previous work has shown that aromatic amines in aqueous solution can effectively eject an electron from the excited singlet state and that the localized positive charge on the nitrogen was a key factor in their photoionization[27]. Based upon the observations in this work that FLU primarily reacts from a singlet state, and a pKa of 12.3 resulting in the quaternary amine being the primary form of FLU under environmentally relevant conditions, Pathway II is likely a major contributor to the overall photochemical degradation observed in this work and others. Pathway III: photohydration and ring opening of the pyridinone ring, either directly from FLU or following the loss of the phenyl group, resulted in another major photoproduct - trifluoromethyl benzoic acid ($C_8H_5F_3O_2$) (Figure 6). Reaction with ·OH also

resulted in minor formation of oxidized photoproducts following phenyl ring opening in Pathway IV, such as $C_{15}H_{12}F_3NO_2$ (Figure 6 & Supporting Information for Transformation Products); however, these products were less abundant than those observed for Pathways I-III. Observed intermediates for Pathways I, III, and IV were primarily formed via reaction at or nearer the non-substituted phenyl ring, consistent with the deactivating tendency of strongly electron withdrawing trifluoromethyl substitution on aromatic rings.

Peak area vs time trends for major photoproducts (Figure 7) revealed further insights into the photodegradation mechanism. Larger intermediates ($C_{17\text{-}19}$) maintaining multiple aromatic chromophores generally peaked in the first 24 hrs, then degraded by the end of the treatment (4-8 days). This was especially true for the N-demethylated product $C_{18}H_{12}F_3NO$ formed in the direct treatment, which was both rapidly formed and converted to other compounds (Figure 7). Mid-size intermediates (e.g., $C_{12}H_{11}NO$, $C_{13}H_{10}F_3NO$, $C_{15}H_{12}F_3NO_2$) continued to form in the direct treatment as FLU continued to degrade, but generally depleted after 24 hr in the NO_3^- treatment; suggesting that pyridinone ring opening to further products (Supporting Information for Transformation Products) is accelerated by ·OH. Smaller photoproducts ($C_{5\text{-}9}$, e.g., $C_8H_5F_3O_2$) typically plateaued (or reached a steady-state) after 4 days of exposure, showing signs of further degradation sooner in the NO_3^- treatment; consistent with indirect photochemistry beginning to dominate as the aromatic chromophoric structures in FLU are sequentially decomposed. Additional products gained -NO_3 functional groups (Supporting Information for Transformation Products) and continued to increase in concentration over the duration of the experiment. These compounds are attributed to reaction with nitrate radical[37], and are not included in our discussion because they are unlikely to form under environmentally relevant NO_3^- concentrations.

Previous studies identified similar photoproducts, along with additional small polar final products that were not the target of our approach to capture a broad picture of unidentified intermediates that would help elucidate degradation pathways. Muir et al. (1982) identified desphenylfluridone ($C_{13}H_{10}F_3NO$, Figure 6) as a major photoproduct, with extensive further degradation to unextractable (w/ dichloromethane under acidic conditions) polar products being the major degradation pathway[45]. Saunders and Mosier (1983) conducted a more extensive study of fluridone photoproducts, also identifying the ring loss $C_{13}H_{10}F_3NO$ and $C_{12}H_{11}NO$ (Figure 6) but not in significant quantities, postulating that they were as photolabile as fluridone[22]. This work identifies multiple pyridinone ring opening products of the desphenyl- and destrifluoromethylphenyl- fluridone intermediates (Figure 6 & Supporting Information for Transformation Products) that support this hypothesis; however, the Pathway I intermediates were observed to plateau in systems where $[\cdot OH]_{ss}$ was low, suggesting that they are less photolabile than the parent FLU structure (Figure 7). Benzoic acid ($C_7H_6O_2$) and 3-(trifluoromethyl)-benzoic acid ($C_8H_5F_3O_2$), also observed in this study (Figure 6), along with benzaldehyde (C_7H_6O), 3-(trifluoro-methyl)benzaldehyde ($C_8H_5F_3O$), and N-methylformamide (NMF, C_2H_5NO) were identified as primary products, along with significant volatilization losses. While it is impossible to quantify these compounds without primary standards, decreasing recovery of photoproducts over time in this work suggests the formation of smaller polar or volatile photoproducts (such as NMF) not captured by SPE. These photoproducts suggested a mechanism involving the complete degradation of the pyridinone ring, similar to results from Shim (1967) who proposed that the photolysis of N-methyl-4-pyridinone proceeded by hydration

α to nitrogen followed by ring opening, though photoproducts could not be isolated in their study[46]. Other studies searched for the formation of NMF in treated waters without success, despite it being a primary photoproduct in lab studies[47–49]. Pyridinone ring opening pathways observed in this study reveal potential mechanisms for the formation of NMF (*e.g.,* Pathway III. $C_{17}H_{11}F_3O_3$; Figure 6); however, multiple N-demethylated pyridinone ring opening products were observed that preclude the exclusive formation of NMF and support its absence as a major observed photoproduct (*e.g.,* Pathway III. $C_{10}H_8F_3NO$; Figure 6).

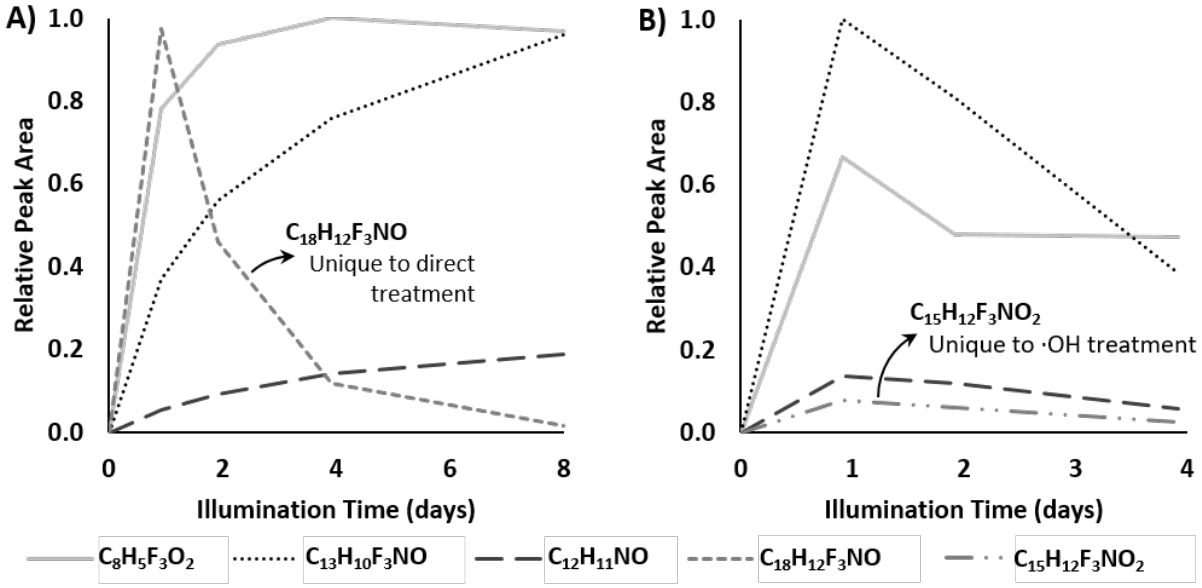

Figure 7. Relative peak area vs illumination time for the primary FLU photoproducts observed in the buffered direct (A) and ·OH producing (B) systems. $C_8H_5F_3O_2$, $C_{13}H_{10}F_3NO$, and $C_{12}H_{11}NO$ appear in both systems, while $C_{18}H_{12}F_3NO$ and $C_{15}H_{12}F_3NO_2$ were unique to the direct and ·OH treatments, respectively.

Environmental Implications

This work quantifies the temperature dependence of FLU photochemical degradation, with significantly slower degradation at lower temperatures providing a potential explanation for the observed longer residence times of this aquatic herbicide in high latitude environments. Activation energies measured in this work indicate that as temperature decreases, reactions with ·OH may begin to contribute more to the overall degradation of FLU than direct photochemical processes. Therefore, the interplay between light screening and ·OH production by CDOM will likely result in site specific relevance of this pathway compared to direct photochemical degradation. Pathways for the processes responsible for these kinetics were determined via non-target analysis to aid in the interpretation of reaction mechanisms and identification of transformation products that may accumulate as FLU degrades. Four primary

degradation pathways were identified with one unique to direct photochemistry (Pathway II: N-demethylation), one unique to reaction with ·OH (Pathway IV: Phenyl ring opening), and two common to both (Pathways I & III: biphenyl bond cleavage and photo hydrolytic pyridinone ring opening). Photoproducts identified during this study can also facilitate future work on the persistence and toxicity of FLU degradation products in aquatic environments.

Associated Content

Supporting Information (docx): Chemical reagents. Photodegradation experiment details. 2NB actinometry rate constants. Quantitative methods for FLU, PhOH, and 2NB including MS/MS acquisition parameters. Description of solid phase extraction and identification of FLU photoproducts by UHPLC-Orbitrap non-target analysis. Tabulated absorptivity values for FLU. Tabulated rate constants for the degradation of FLU in experimental treatments. Activation energy, enthalpy of activation, and entropy of activation for the degradation of FLU.

Supporting Information for Transformation Products (xlsx): Complete transformation pathway of FLU photochemical degradation intermediates/products. Tabulated summary of photoproducts identified. Compilation of UHPLC-Orbitrap chromatograms, MS2 spectra and fragmentation data, and chromatogram peak area vs time data for each photoproduct.

Funding

Research reported in this publication was supported by the National Science Foundation award 2203761.

Notes

The authors declare no competing financial interest.

Acknowledgements

We thank L Wieland for analytical instrumentation support in the University of Alaska Anchorage Applied Science, Engineering and Technology Lab (UAA ASET) throughout this project.

References

(1) Conn, J. S.; Cameron, J. S. Persistence and Carry-over of Metribuzin and Triallate in Subarctic Soils. *Can. J. Soil Sci.* **1988**, *68* (4), 827–830. https://doi.org/10.4141/cjss88-082.
(2) Tomco, P. L.; Duddleston, K. N.; Schultz, E. J.; Hagedorn, B.; Stevenson, T. J.; Seefeldt, S. S. Field Degradation of Aminopyralid and Clopyralid and Microbial Community Response to Application in Alaskan Soils. *Environ. Toxicol. Chem.* **2016**, *35* (2), 485–493. https://doi.org/10.1002/etc.3222.

(3) Barnes, D. D. L.; Seefeldt, D. S. Attenuation and Effectiveness of Triclopyr and 2, 4-D Along Alaska Highway Right-of-Way in a Continental and a Costal Subarctic Environment.
(4) Seefeldt, S. S.; Boydston, R. A.; Kaspari, P. N.; Zhang, M.; Carr, E.; Smeenk, J.; Barnes, D. L. Aminopyralid Residue Impacts on Potatoes and Weeds. *Am. J. Potato Res.* **2013**, *90* (3), 239–244. https://doi.org/10.1007/s12230-012-9298-4.
(5) Newton, M.; Cole, E. C.; Tinsley, I. J. Dissipation of Four Forest-Use Herbicides at High Latitudes. *Environ. Sci. Pollut. Res.* **2008**, *15* (7), 573–583. https://doi.org/10.1007/s11356-008-0039-7.
(6) Rahel, F. J.; Olden, J. D. Assessing the Effects of Climate Change on Aquatic Invasive Species. *Conserv. Biol.* **2008**, *22* (3), 521–533. https://doi.org/10.1111/j.1523-1739.2008.00950.x.
(7) Bellard, C.; Thuiller, W.; Leroy, B.; Genovesi, P.; Bakkenes, M.; Courchamp, F. Will Climate Change Promote Future Invasions? *Glob. Change Biol.* **2013**, *19* (12), 3740–3748. https://doi.org/10.1111/gcb.12344.
(8) Morton, J. M.; Blackburn, B. N.; Bella, E.; Steffy, M.; Anderson, C.; Massengill, R.; Blackwell, J.; Ka'aihue, L.; Zulueta, R.; Chumley, J.; Aranquiz, M.; Rich, C. *Integrated Pest Management Plan for Eradication Elodea from the Kenai Peninsula*; Elodea Subcommittee of the Kenai Peninsula Cooperative Weed Management Area; p 45.
(9) Morton, J. M.; Coleman, D. P.; Schake, K.; Blackwell, J.; Bornemann, B.; Graham, K.; Hester, J.; Ka'aihue, L.; Massengill, R.; Ahlberg, B.; Martin, A.; Bowser, M. *Integrated Pest Management Plan for Eradicating Elodea*; version 7; Elodea Committee of the Kenai Peninsula Cooperative Invasive Species Management Area, 2021; p 93.
(10) Shaner, D. L. *Herbicide Handbook*, 10th Edition.; Weed Science Society of America, 2014.
(11) Van Frost, S. R.; White, A. M.; Jauquet, J. M.; Magness, A. M.; McMahon, K. D.; Remucal, C. K. Laboratory Measurements Underestimate Persistence of the Aquatic Herbicide Fluridone in Lakes. *Environ. Sci. Process. Impacts* **2024**, *26* (2), 368–379. https://doi.org/10.1039/D3EM00537B.
(12) Macdonald, G. E.; Haller, W. T.; Shilling, D. G. UV-B Filtration to Reduce Photolysis of Fluridone in Experimental Tanks. *J Aquat Plant Manage* **1996**, *34* (2), 78–80.
(13) Mossler, M. A.; Shilling, D. G.; Haller, W. T. Photolytic Degradation of Fluridone. *J Aquat Plant Manage* **1989**, *27*, 69–73.
(14) Locatelli, M.; Carlucci, G.; Genovese, S.; Curini, M.; Epifano, F. Use of HPLC in the Determination of the Molar Absorptivity of 4′-Geranyloxyferulic Acid and Boropinic Acid. *Chromatographia* **2011**, *73* (9–10), 889–896. https://doi.org/10.1007/s10337-011-1979-5.
(15) Pelillo, M.; Cuvelier, M. E.; Biguzzi, B.; Gallina Toschi, T.; Berset, C.; Lercker, G. Calculation of the Molar Absorptivity of Polyphenols by Using Liquid Chromatography with Diode Array Detection: The Case of Carnosic Acid. *J. Chromatogr. A* **2004**, *1023* (2), 225–229. https://doi.org/10.1016/S0021-9673(03)01206-8.
(16) Redman, Z.; Begley, J.; Hillestad, I.; Tomco, P. Reactive Oxygen Species and Chromophoric Dissolved Organic Matter Drive the Aquatic Photochemical Pathways and Photoproducts of 6PPD-Quinone under Simulated High-Latitude Conditions. *Environ. Sci. Technol.* **2023**, *57* (49), 20813–20821. https://doi.org/10.1021/acs.est.3c05742.
(17) Galbavy, E. S.; Ram, K.; Anastasio, C. 2-Nitrobenzaldehyde as a Chemical Actinometer for Solution and Ice Photochemistry. *J. Photochem. Photobiol. Chem.* **2010**, *209* (2–3), 186–192. https://doi.org/10.1016/j.jphotochem.2009.11.013.
(18) Haag, W. R.; Yao, C. C. D. Rate Constants for Reaction of Hydroxyl Radicals with Several Drinking Water Contaminants. *Environ. Sci. Technol.* **1992**, *26* (5), 1005–1013. https://doi.org/10.1021/es00029a021.
(19) Latch, D. E.; Stender, B. L.; Packer, J. L.; Arnold, W. A.; McNeill, K. Photochemical Fate of Pharmaceuticals in the Environment: Cimetidine and Ranitidine. *Environ. Sci. Technol.* **2003**, *37* (15), 3342–3350. https://doi.org/10.1021/es0340782.

(20) Lipczynska-Kochany, E.; Sprah, G.; Harms, S. Influence of Some Groundwater and Surface Waters Constituents on the Degradation of 4-Chlorophenol by the Fenton Reaction. *Chemosphere* **1995**, *30* (1), 9–20. https://doi.org/10.1016/0045-6535(94)00371-Z.
(21) Lv, M.; Wang, X.; Pan, H.; Chen, J. Direct Observation of Ultrafast Access to a Solvent-Independent Singlet–Triplet Equilibrium State in Acridone Solutions. *J. Phys. Chem. B* **2021**, *125* (48), 13291–13297. https://doi.org/10.1021/acs.jpcb.1c08844.
(22) Saunders, D. G.; Mosier, J. W. Photolysis of the Aquatic Herbicide Fluridone in Aqueous Solution. *J. Agric. Food Chem.* **1983**, *31* (2), 237–241. https://doi.org/10.1021/jf00116a013.
(23) Innes, K. K. Photochemistry: Threshold Frequencies and Temperature Dependence of Primary Processes. *J. Chem. Educ.* **1965**, *42* (2), 109. https://doi.org/10.1021/ed042p109.
(24) Zellner, R.; Exner, M.; Herrmann, H. Absolute OH Quantum Yields in the Laser Photolysis of Nitrate, Nitrite and Dissolved H2O2 at 308 and 351 Nm in the Temperature Range 278?353 K. *J. Atmospheric Chem.* **1990**, *10* (4), 411–425. https://doi.org/10.1007/BF00115783.
(25) Chu, L.; Anastasio, C. Quantum Yields of Hydroxyl Radical and Nitrogen Dioxide from the Photolysis of Nitrate on Ice. *J. Phys. Chem. A* **2003**, *107* (45), 9594–9602. https://doi.org/10.1021/jp0349132.
(26) McKay, G.; Rosario-Ortiz, F. L. Temperature Dependence of the Photochemical Formation of Hydroxyl Radical from Dissolved Organic Matter. *Environ. Sci. Technol.* **2015**, *49* (7), 4147–4154. https://doi.org/10.1021/acs.est.5b00102.
(27) Saito, F.; Tobita, S.; Shizuka, H. Photoionization Mechanism of Aniline Derivatives in Aqueous Solution Studied by Laser Flash Photolysis. *J. Photochem. Photobiol. Chem.* **1997**, *106* (1–3), 119–126. https://doi.org/10.1016/S1010-6030(97)00048-8.
(28) Workentin, M. S.; Schepp, N. P.; Johnston, L. J.; Wayner, D. D. M. Solvation Control of Chemoselectivity in Reactions of Radical Cations. *J. Am. Chem. Soc.* **1994**, *116* (3), 1141–1142. https://doi.org/10.1021/ja00082a050.
(29) Wang, J.; Wang, S. Reactive Species in Advanced Oxidation Processes: Formation, Identification and Reaction Mechanism. *Chem. Eng. J.* **2020**, *401*, 126158. https://doi.org/10.1016/j.cej.2020.126158.
(30) Alfassi, Z. B.; Harriman, Anthony.; Huie, R. E.; Mosseri, S.; Neta, P. The Redox Potential of the Azide/Azidyl Couple. *J. Phys. Chem.* **1987**, *91* (8), 2120–2122. https://doi.org/10.1021/j100292a029.
(31) Alfassi, Z. B.; Schuler, R. H. Reaction of Azide Radicals with Aromatic Compounds. Azide as a Selective Oxidant. *J. Phys. Chem.* **1985**, *89* (15), 3359–3363. https://doi.org/10.1021/j100261a040.
(32) Shee, M.; Singh, N. D. P. Chemical Versatility of Azide Radical: Journey from a Transient Species to Synthetic Accessibility in Organic Transformations. *Chem. Soc. Rev.* **2022**, *51* (6), 2255–2312. https://doi.org/10.1039/D1CS00494H.
(33) Reszka, K.; Hall, R. D.; Chignell, C. F. Quenching of the Excited States of 2-Phenylbenzoxazole by Azide Anion. Fluorescence and ESR Study. *Photochem. Photobiol.* **1984**, *40* (6), 707–714. https://doi.org/10.1111/j.1751-1097.1984.tb04641.x.
(34) Wan, P.; Culshaw, S.; Yates, K. Photohydration of Aromatic Alkenes and Alkynes. *J. Am. Chem. Soc.* **1982**, *104* (9), 2509–2515. https://doi.org/10.1021/ja00373a029.
(35) Davis, C. A.; McNeill, K.; Janssen, E. M.-L. Non-Singlet Oxygen Kinetic Solvent Isotope Effects in Aquatic Photochemistry. *Environ. Sci. Technol.* **2018**, *52* (17), 9908–9916. https://doi.org/10.1021/acs.est.8b01512.
(36) Haag, W. R.; Hoigné, J. Photo-Sensitized Oxidation in Natural Water via .OH Radicals. *Chemosphere* **1985**, *14* (11–12), 1659–1671. https://doi.org/10.1016/0045-6535(85)90107-9.

(37) Zepp, R. G.; Hoigne, Juerg.; Bader, Heinz. Nitrate-Induced Photooxidation of Trace Organic Chemicals in Water. *Environ. Sci. Technol.* **1987**, *21* (5), 443–450. https://doi.org/10/cwj9th.
(38) Mopper, K.; Zhou, X. Hydroxyl Radical Photoproduction in the Sea and Its Potential Impact on Marine Processes. *Science* **1990**, *250* (4981), 661–664. https://doi.org/10.1126/science.250.4981.661.
(39) Brezonik, P. L.; Fulkerson-Brekken, J. Nitrate-Induced Photolysis in Natural Waters: Controls on Concentrations of Hydroxyl Radical Photo-Intermediates by Natural Scavenging Agents. *Environ. Sci. Technol.* **1998**, *32* (19), 3004–3010. https://doi.org/10.1021/es9802908.
(40) Vione, D.; Falletti, G.; Maurino, V.; Minero, C.; Pelizzetti, E.; Malandrino, M.; Ajassa, R.; Olariu, R.-I.; Arsene, C. Sources and Sinks of Hydroxyl Radicals upon Irradiation of Natural Water Samples. *Environ. Sci. Technol.* **2006**, *40* (12), 3775–3781. https://doi.org/10.1021/es052206b.
(41) Schymanski, E. L.; Jeon, J.; Gulde, R.; Fenner, K.; Ruff, M.; Singer, H. P.; Hollender, J. Identifying Small Molecules via High Resolution Mass Spectrometry: Communicating Confidence. *Environ. Sci. Technol.* **2014**, *48* (4), 2097–2098. https://doi.org/10.1021/es5002105.
(42) Ripper, J. A.; Tiekink, E. R. T.; Scammells, P. J. Photochemical N-Demethylation of Alkaloids. *Bioorg. Med. Chem. Lett.* **2001**, *11* (4), 443–445. https://doi.org/10.1016/S0960-894X(00)00690-9.
(43) Santamaria, J.; Ouchabane, R.; Rigaudy, J. Electron-Transfer Activation. Photochemical N-Demethylation of Tertiary Amines. *Tetrahedron Lett.* **1989**, *30* (22), 2927–2928. https://doi.org/10.1016/S0040-4039(00)99160-3.
(44) Lee, L. Y. C.; Ci, Xiaohong.; Giannotti, Charles.; Whitten, D. G. Photoinduced Carbon-Carbon Bond Cleavage via Electron-Transfer Reactions: Visible-Light-Mediated Scission of Tertiary Amines. *J. Am. Chem. Soc.* **1986**, *108* (1), 175–177. https://doi.org/10.1021/ja00261a029.
(45) Muir, D. C. G.; Grift, N. P. Fate of Fluridone in Sediment and Water in Laboratory and Field Experiments. *J. Agric. Food Chem.* **1982**, *30* (2), 238–244. https://doi.org/10.1021/jf00110a006.
(46) Shim, S. C. Part Two: Photochemistry of N-Methyl-4-Pyridinone and N-Methyllutidone, California Institute of Technology, 1967.
(47) Osborne, J. A.; West, S. D.; Cooper, R. B.; Schmitz, D. C. Fluridone and N-Methylformamide Residue Determinations in Ponds. *J Aquat Plant Manage* **1989**, *27*, 74–78.
(48) Pfeuffer, R. J. *Herbicide Monitoring Program for N-Methylformamide and Fluridone [Sonar(R)]*; 1990.
(49) West, S. D.; Langeland, K. A.; Laroche, F. B. Residues of Fluridone and a Potential Photoproduct (N-Methylformamide) in Water and Hydrosoil Treated with the Aquatic Herbicide Sonar. *J. Agric. Food Chem.* **1990**, *38* (1), 315–319. https://doi.org/10.1021/jf00091a069.